Magnetic phase diagram of the Kondo lattice model with quantum localized spins

J. Kienert and W. Nolting
Lehrstuhl Festkörpertheorie, Institut für Physik, Humboldt-Universität zu Berlin, Newtonstr. 15, 12489 Berlin, Germany

The magnetic phase diagram of the ferromagnetic Kondo lattice model is determined at T=0 in 1D, 2D, and 3D for various magnitudes of the quantum mechanical localized spins ranging from $S = \frac{1}{2}$ to classical spins ($S \to \infty$). We consider the ferromagnetic phase, the paramagnetic phase, and the ferromagnetic/antiferromagnetic phase separated regime. There is no significant influence of the spin quantum number on the phase boundaries except for the case $S = \frac{1}{2}$, where the model exhibits an instability of the ferromagnetic phase with respect to spin disorder. Our results give support, at least as far as the low temperature magnetic properties are concerned, to the classical treatment of the $S = 3/2-$spins in the intensively investigated manganites, for which the ferromagnetic Kondo-lattice model is generally employed to account for magnetism.

I. INTRODUCTION

The ferromagnetic Kondo lattice model (FKLM), also known as *s-d* model or double exchange model, has drawn a lot of attention over the past years in the field of magnetism and electronic correlations. The model consists of Bloch electrons coupled to localized spins sitting on the sites of a crystal lattice. For the case of strong (Hund) coupling and an energetically favored parallel orientation of a localized moment and an electron, Zener proposed the double exchange mechanism to explain ferromagnetism (FM) in manganites.[1] The gain in kinetic energy of the conduction electrons favors a parallel configuration of the localized spins. In the framework of a two-site model, Anderson and Hasegawa showed that the hopping amplitude of the electrons between sites i and j is proportional to $cos(\theta_{ij}/2)$, where θ_{ij} is the angle between the localized spins.[2]

A major field of application for the FKLM is linked to the phenomenon of colossal magnetoresistance[3] in the manganese compounds already aimed at by Zener. Here, the 5 Mn d-shells are split by the crystal field into three degenerate t_{2g}-orbitals forming localized spins of $S = \frac{3}{2}$. They interact via Hund's rule with itinerant electrons stemming from the remaining two degenerate e_g-orbitals. With a Hund exchange interaction mostly estimated to be several times the hopping amplitude[4,5,6] the manganites belong to the rather strongly coupled materials. Although there are other important aspects to take into account when modelling the rich physics of the manganites, like eletron-phonon-coupling and the second conduction band, the FKLM already in its simplest single band version is crucial for understanding at least the magnetic properties of this class of substances.[6]

A hot topic where the FKLM is used as a basic model are the diluted magnetic semiconductors (DMS) with promising technical applications for microelectronics.[7,8] These materials consist of a (often III/V as, e.g., GaAs) semiconducting host and substituted transition metal impurities (e.g. Mn) occupying cation sites, the latters exhibiting ferromagnetism due to a coupling of the localized cation spins mediated by a spin exchange interaction with valence and impurity band holes. In the case of DMS, this interaction is considered intermediate.[9]

There have been various types of approaches to solving the many-body problem of the FKLM in order to get a phase diagram. On the theoretical side, several treatments are based on Dynamical Mean Field Theory (DMFT).[10,11,12,13] In Ref. 14 a Schwinger-boson method is used and applied to 2D and 3D. Bosonization in 1D is extensively discussed in Ref. 15. More recently an analytical continuum field theory in 2D was employed.[16] Valuable information to compare theoretical results with can be gathered from Monte Carlo simulations.[12,13,17] The main feature of the magnetic phase diagram is the same in all these works: with increasing coupling strength ferromagnetism (FM) prevails for all charge carrier densities except for a more or less small region around half-filling where antiferromagnetism (AFM) or FM/AFM phase separation exists.

Most approaches rely on the assumption that the local spins can be treated classically. This simplification has been justified by checking the classical spin against quantum spin approaches, both giving similar results.[12,13] More recently, a phase diagram in 1D was obtained by means of the Density-Matrix Renormalization Group (DMRG) yielding numerically exact results for a quantum spin $S = 1/2$.[18] However, we do not know of any systematic, quantitative analysis of the influence of the spin magnitude on the magnetic properties of the FKLM.

In this work we present phase diagrams of the FKLM at T=0 for several spin quantum numbers in 1D, 2D, and 3D. We use an equation of motion approach exploiting exactly solvable limiting cases and exact relations among Green functions and among their spectral moments. By evaluating the (free) energy at T=0 we can distinguish three different phases: paramagnetic (PM), ferromagnetic, and ferromagnetic-antiferromagnetic phase separated (PS). The latter two are the typical phases in the strong coupling region of the phase diagram[12,13,14,16,18] which is the regime relevant for the manganites and on which we want to focus in our work. It should be mentioned that in the weak to intermediate coupling regime several other phases like canted, spiral, or island have been found.[14,16,18]

One of the main results will be that there are no ma-

jor differences in the FM-PS phase boundaries for spin quantum numbers $S > 1/2$. The case $S = 1/2$ is special: here we obtain an instability of the ferromagnetic against the paramagnetic phase. To understand this behavior we discuss the spectral weight distribution of the excitation spectrum and its modifications by a variation of the quantum character of the localized spins.

The paper is organized as follows. After presenting our theoretical approach in section II we discuss the phase diagrams of the FKLM in 1D, 2D, and 3D for different quantum numbers of the localized spins in section III. A summary and an outlook on possible improvements of our theory are given in section IV.

II. THEORY

The Hamiltonian of the FKLM reads

$$H = -t \sum_{\langle ij \rangle \sigma} c^\dagger_{i\sigma} c_{j\sigma} - J \sum_i \mathbf{s}_i \cdot \mathbf{S}_i \; . \tag{1}$$

The first term describes Bloch electrons of spin σ with a nearest neighbor hopping integral t. $c^{(\dagger)}_{i\sigma}$ annihilates (creates) an electron of spin σ at lattice site i. The lattice is chosen to be simple cubic in our case. $\mathbf{s}$ is the electron spin and $\mathbf{S}$ the localized spin operator, and both are coupled through a Hund exchange J. Using standard second quantization notation the interaction term can be rewritten

$$H_{int} = -\frac{1}{2} J \sum_{i\sigma} z_\sigma S^z_i n_{i\sigma} + S^{-\sigma}_i c^\dagger_{i\sigma} c_{i-\sigma} \tag{2}$$

with $z_{\uparrow,\downarrow} = \pm 1$, $S^{z,+,-}_i$ are the z-component, raising and lowering operators for a localized spin at site i, and $n_{i\sigma} = c^\dagger_{i\sigma} c_{i\sigma}$ is the occupation number operator at site i.

The many-body problem of the above Hamiltonian is solved with the knowledge of the one-electron Green function $G_{\mathbf{k}\sigma}(E)$, or, equivalently, the electronic self-energy $\Sigma_{\mathbf{k}\sigma}(E)$:

$$\begin{aligned} G_{ij\sigma}(E) &= \langle\langle c_{i\sigma}; c^\dagger_{j\sigma} \rangle\rangle_E = \frac{1}{N} \sum_{\mathbf{k}} G_{\mathbf{k}\sigma}(E) e^{i\mathbf{k}(\mathbf{R}_i - \mathbf{R}_j)} \; , \\ G_{\mathbf{k}\sigma}(E) &= \frac{\hbar}{E - \epsilon(\mathbf{k}) - \Sigma_{\mathbf{k}\sigma}(E)} \; , \end{aligned} \tag{3}$$

with the Bloch dispersion $\epsilon(\mathbf{k})$. One can then calculate the internal energy U of the FKLM, being equivalent to the free energy at T=0, for the ferromagnetic and the paramagnetic state. There is a simple relation between the energy U of the FKLM and the imaginary part of the corresponding one-particle Green function,

$$U = \langle H \rangle = \frac{1}{N\hbar} \sum_{i\sigma} \int_{-\infty}^{+\infty} dE f_-(E) E S_{ii\sigma}(E) \; , \tag{4}$$

where $S_{ii\sigma}(E) = -\frac{1}{\pi} \Im G_{ii\sigma}(E)$ is the local spectral density and f_- denotes the Fermi function.[19]

Note that the existence of the ferromagnetic state is supposed and not the result of a self-consistent calculation, i.e. the magnetization is a parameter in our scheme.

The method we chose to solve the Hamiltonian (1) for the Green function (3) is a moment conserving decoupling approach (MCDA), which does *not* require the localized spins to be classical. This theory has been applied before in model studies[20] and to real substances[21,22]. For a detailed account of the decoupling procedure we refer the reader to Ref.[23]. Here we summarize the main points of the method and want to emphasize features which are important for the following discussion of our results.

The starting point is the equation of motion for the Green function (3). The generated higher Green functions read

$$I_{ik,j\sigma}(E) = \langle\langle S^z_i c_{k\sigma}; c^\dagger_{j\sigma} \rangle\rangle_E \; , \tag{5}$$

$$F_{ik,j\sigma}(E) = \langle\langle S^{-\sigma}_i c_{k-\sigma}; c^\dagger_{j\sigma} \rangle\rangle_E \; . \tag{6}$$

$I_{ik,j\sigma}(E)$ is a Ising-like GF solely comprising the z-components of the spins, whereas $F_{ik,j\sigma}(E)$ describes spin flip processes which are neglected when using classical localized spins. After writing down the equations of motion of $I_{ik,j\sigma}(E)$ and $F_{ik,j\sigma}(E)$ the decoupling is performed. Of special importance for correlation effects is the treatment of the local higher Green functions, namely

$$F^{(1)}_{ii,j\sigma}(E) = \langle\langle S^{-\sigma}_i S^z_i c_{i-\sigma}; c^\dagger_{j\sigma} \rangle\rangle_E \; , \tag{7}$$

$$F^{(2)}_{ii,j\sigma}(E) = \langle\langle S^{-\sigma}_i S^\sigma_i c_{i\sigma}; c^\dagger_{j\sigma} \rangle\rangle_E \; , \tag{8}$$

$$F^{(3)}_{ii,j\sigma}(E) = \langle\langle S^{-\sigma}_i n_{i\sigma} c_{i-\sigma}; c^\dagger_{j\sigma} \rangle\rangle_E \; , \tag{9}$$

$$F^{(4)}_{ii,j\sigma}(E) = \langle\langle S^z_i n_{i-\sigma} c_{i\sigma}; c^\dagger_{j\sigma} \rangle\rangle_E \; . \tag{10}$$

These functions are expressed in terms of the lower order GF (3), (5), and (6) with coefficients fitted by the first two spectral moments of these GFs, respectively, representing a non-perturbative approximation for the whole temperature range.[23] The choice of the "correct" lower order GF is guided by some non-trivial limiting cases which we summarize next.

For an assumed complete ferromagnetic polarization ($\langle S^z \rangle = S$) of the FKLM one obtains from the spectral representation of the Green functions:

$$F^{(1)}_{ii,j\sigma}(E) \overset{\langle S^z \rangle = S}{=} \left(\left(S - \frac{1}{2} \right) + \frac{1}{2} z_\sigma \right) F_{ii,j\sigma}(E) \; , \tag{11}$$

$$F^{(2)}_{ii,j\sigma}(E) \overset{\langle S^z \rangle = S}{=} S G_{ij\sigma}(E) - z_\sigma I_{ii,j\sigma}(E) \; . \tag{12}$$

For $S = \frac{1}{2}$, a case which is of particular importance to our investigation due to its maximum amount of quantum fluctuations, the following relations hold at any temperature (i.e. at any $\langle S_z \rangle$):

$$F^{(1)}_{ii,j\sigma}(E) \overset{S=\frac{1}{2}}{=} \frac{1}{2} z_\sigma F_{ii,j\sigma}(E) \; , \tag{13}$$

$$F^{(2)}_{ii,j\sigma}(E) \overset{S=\frac{1}{2}}{=} \frac{1}{2} G_{ij\sigma}(E) - z_\sigma I_{ii,j\sigma}(E) \; . \tag{14}$$

Furthermore in the case of a fully occupied conduction band:

$$F^{(3)}_{ii,j\sigma}(E) \stackrel{n=2}{=} F_{ii,j\sigma}(E)\ , \tag{15}$$

$$F^{(4)}_{ii,j\sigma}(E) \stackrel{n=2}{=} I_{ii,j\sigma}(E)\ . \tag{16}$$

The above exact relations are used to motivate the following ansatz for the higher local GF:

$$F^{(1)}_{ii,j\sigma}(E) = \alpha_{1\sigma}G_{ij\sigma}(E) + \beta_{1\sigma}F_{ii,j\sigma}(E)\ , \tag{17}$$

$$F^{(2)}_{ii,j\sigma}(E) = \alpha_{2\sigma}G_{ij\sigma}(E) + \beta_{2\sigma}I_{ii,j\sigma}(E)\ , \tag{18}$$

$$F^{(3)}_{ii,j\sigma}(E) = \alpha_{3\sigma}G_{ij\sigma}(E) + \beta_{3\sigma}F_{ii,j\sigma}(E)\ , \tag{19}$$

$$F^{(4)}_{ii,j\sigma}(E) = \alpha_{4\sigma}G_{ij\sigma}(E) + \beta_{4\sigma}I_{ii,j\sigma}(E)\ . \tag{20}$$

The temperature dependent interpolation coefficients $\alpha_{i\sigma},\ \beta_{i\sigma}$ $(i = 1, .., 4)$ depend on various correlation functions and are listed in Appendix A. It is easily verified that the approximations (17)-(20) fulfill the exact limiting cases (11)-(16). In addition our approach reproduces the limit of the ferromagnetically saturated semiconductor (T=0, band occupation n=0).[24]

The resulting self-energy $\Sigma_\sigma(E)$ is local and depends on various expectation values of pure fermionic, mixed fermionic-spin, and pure localized spin character:

$$\Sigma_\sigma = F(\langle n_\sigma\rangle, \langle S^{-\sigma}c^\dagger_\sigma c_{-\sigma}\rangle,\ \langle S^z n_\sigma\rangle, \langle S^z\rangle,\ \langle (S^z)^2\rangle,\ \langle (S^z)^3\rangle,\ \langle S^+S^-\rangle)\ . \tag{21}$$

The site indices have been dropped due to translational invariance. Whereas the first two types can be calculated within the MCDA the localized spin correlation functions are known for ferromagnetic saturation and in the paramagnetic state (see Appendix B). The many-body problem represented by (1) can thus be solved approximately for the Green function (3) in a self-consistent manner.[23] We emphasize that the quantum mechanical character of the localized spins is fully retained in our approach. Furthermore there is no restriction to the parameter range within which our method can be applied.

In order to determine the phase boundary between the ferromagnetic and the ferromagnetic-antiferromagnetic phase separated region we first have to solve the Hamiltonian (1) for an antiferromagnetic configuration. Using the standard sublattice decomposition for bipartite lattices and neglecting the off-diagonal elements of the self-energy matrix[25] one obtains the following Green function for sublattice A:

$$G^A_{\mathbf{k}\sigma}(E) = \frac{\hbar}{E - \epsilon'(\mathbf{k}) - \Sigma^A_{\mathbf{k}\sigma}(E) - \frac{|t(\mathbf{k})|^2}{E-\epsilon'(\mathbf{k})-\Sigma^B_{\mathbf{k}\sigma}(E)}} \tag{22}$$

with the diagonal elements of the self-energy matrix $\Sigma^A_{\mathbf{k}\sigma} = \Sigma^B_{\mathbf{k}-\sigma}$, the sublattice dispersion $\epsilon'(\mathbf{k})$ and the inter-sublattice dispersion $t(\mathbf{k})$. The approximate solution for the self-energy presented above for the translationally invariant case can be obtained analogously for the antiferromagnetic case. The energy of the antiferromagnetic phase can be evaluated using (4) by simply replacing $S_{ii\sigma}(E)$ by $S^A_{ii\sigma}(E)$. Averaging over the sublattices is not necessary due to symmetry reasons, i.e. the summation over the sublattices is absorbed into the spin summation.

In this work we restrict our considerations concerning AFM to G-type antiferromagnetism, i.e. the spins of all nearest neighbors of a given lattice site belong to the other sublattice. This kind of antiferromagnetism is typical in the strong coupling regime at and near half-filling because it allows for a maximum kinetic energy gain by virtual hopping processes, unlike a FM configuration which forbids these by Pauli's Principle. We assume the ground state has Néel structure, i.e. we set the two magnetic sublattices to be saturated, $\langle S^A_z\rangle = S = -\langle S^B_z\rangle$. Furthermore we do not take into account possible canted AFM configurations.

We used the method proposed in Ref. 14 to determine the FM/PS phase boundary.[26] This criterium for electronic phase separation is based on the separation into AFM regions with one electron at each site and FM domains with an occupation n_c, a picture suggested by numerical results in Ref. 13. On increasing n the AFM part grows until it occupies the whole system at half-filling. The total energy can be written as

$$U_{tot}(n, v) = (1 - v)U_{AFM} + vU_{FM}\left(1 - \frac{1-n}{v}\right) \tag{23}$$

where U_{tot} is the total energy per site, U_{FM} is the FM energy per site and its argument is the particle density in the FM regions (n is the total particle density), U_{AFM} is the AFM energy per site, and $v = V_{FM}/V_{tot}$ is the FM volume fraction of the total system size. Minimizing the total energy with respect to v yields the following condition for the critical electron density n_c at which electronic phase separation sets in (i.e. $v = 1$):

$$U_{AFM} = U_{FM}(n_c) + (1 - n_c)U'_{FM}(n_c)\ . \tag{24}$$

U'_{FM} is the derivative of U_{FM} with respect to the particle density. Note that we consider the electron density and not the hole density in the FKLM so that the corresponding formula in Ref. 14 is modified accordingly.

If one varies the chemical potential μ continuously the electron densities at which phase separation is present correspond to band occupations that cannot be stabilized as, e.g., demonstrated in the MC simulations in Ref. 13. Given the jump in the electron density on varying μ this kind of transition appears to be first-order. However, *enforcing* any value of n as in our case and having in mind the picture of AFM regions gradually taking over the whole system the transition from FM to AFM rather appears to be continuous.

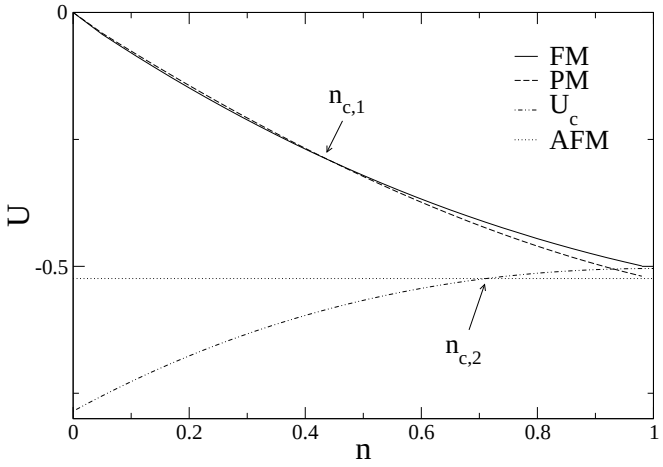

FIG. 1: Total energy (in eV) for ferromagnetic, paramagnetic, and antiferromagnetic configuration for the square lattice. The AFM energy is evaluated at $n = 1$. U_c is computed according to the right hand side of Eq. (24). Parameters: $S = 1/2,\ JS/t = 12$.

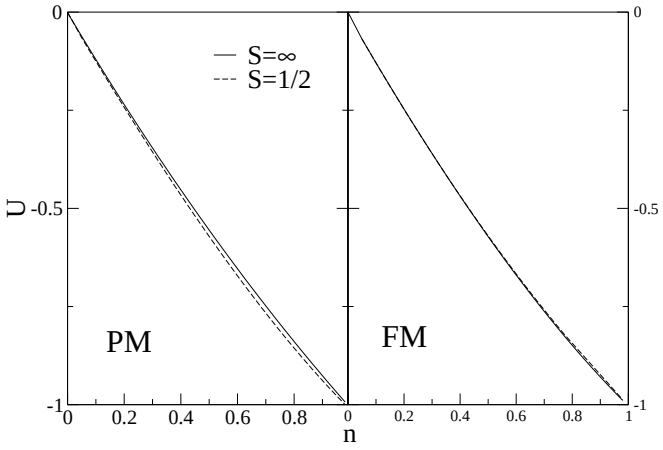

FIG. 2: PM (left) and FM (right) total energy (eV) of the square lattice for quantum $S = 1/2$ and classical localized spins. Parameters: $JS/t = 24$.

III. RESULTS AND DISCUSSION

We computed phase diagrams for different spin quantum numbers S for a simple cubic lattice, a square lattice, and a 1D chain at zero temperature. To simulate a classical spin, i.e. a spin that can be oriented in any direction in space, we used a spin quantum number $S = 10$. In order to obtain a FM-PM-PS phase diagram we evaluated the total energy at T=0 for the saturated ferromagnetic, for the paramagnetic, and for the antiferromagnetic ($n = 1$) spin configuration of the core spins, respectively, as a function of the occupation number n and for several values of the Hund coupling J. To compare the results for different S we take the proper scaling $\propto JS$ of the interaction into account and normalize the localized spins. Thus in the following we consider localized spins $\mathbf{S}/S$ coupled to itinerant electrons by JS.

Before starting the discussion of our results we should add two remarks. First, it is well known that 1D systems exhibit some pecularities; for example, an integer spin nearest-neighbor Heisenberg chain has a gap in its excitation spectrum (*Haldane gap*). Moreover, non-local correlations are important, whereas our approach is based on a local self-energy. However, our approximate theory is applicable for any finite dimension and thus we consider it worthwhile to present results for $D = 1$, too.

Secondly, we have to address the issue of anisotropy. The Mermin-Wagner theorem[27] forbids spontaneous symmetry breaking in $D < 3$ for an isotropic Hamiltonian like (1) at finite temperatures. In order for our results to be relevant at small temperatures, too, we have to add an (infinitesimally) small anisotropy term, e.g. a single-ion anisotropy taking spin orbit coupling into account. Being orders of magnitude smaller than the leading energy scale in our system, the Hund coupling J, it will not alter the phase boundaries visibly. There is another benefit of adding an anisotropy to (1). On decreasing S the assumption of a Néel state for the antiferromagnetic phase becomes questionable due to quantum fluctuations. In 1D this approximation even breaks down completely. These fluctuations are suppressed by anisotropy.[28]

Fig. 1 shows the total energy of the FM and PM phases as a function of the band occupation n and of the AFM phase at $n = 1$. The result of the right hand side of Eq. (24) is also plotted. The spin is $S = 1/2$ corresponding to a maximum of quantum fluctuations. The paramagnetic ground state at $n_{c,1} = 0.45$ emerges well before the criterium (24) for PS is fulfilled at $n_{c,2} = 0.72$, indicating an instability of ferromagnetism against spin disorder. In our calculations we did not find a second transition from PM to PS for $S = 1/2$ at $n > n_{c,1}$. On the other hand for $S \geq 1$ and the values of J we considered ($JS/t \geq 6$) we find that the critical value of n for the onset of phase separation is always lower than the electron density where FM becomes unstable against PM, i.e. $n_{c,2} < n_{c,1}$.

To further analyse the FM-PM transition for $S = 1/2$ we show in Fig. 2 more results for the total energy and compare them to calculations based on classical localized spins. Whereas the PM energy is lower for the quantum spin over the whole range of electron densities the FM energies are practically the same for both spins.

This can be related to the quasiparticle excitation spectrum. As can be seen by (4) the total energy of the FKLM is determined in complete formal analogy to the free electron case, i.e. by the (quasiparticle) density of states. Our findings suggest the following picture: In the FM phase there is a parallel alignment of the conduction electrons with respect to the localized spins. Given a saturated FM spin background it is not possible for an itinerant electron to flip its spin by spin exchange. There is no significant occupation in the $\downarrow$-band of the spectrum for any S. This is, at least for high Hund coupling, consistent with the excitation spectra we obtained (see FM

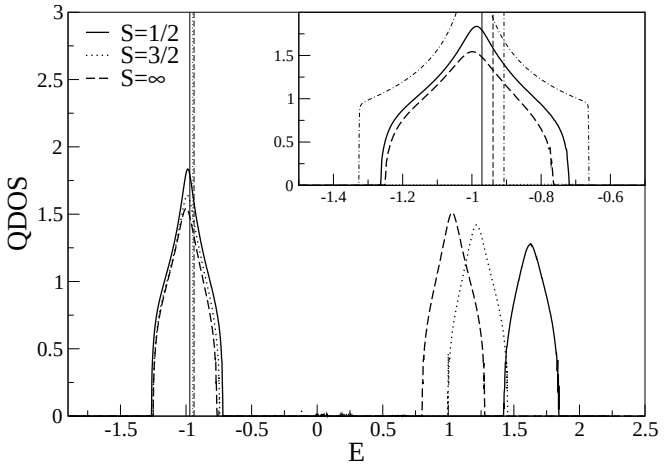

FIG. 3: Paramagnetic quasiparticle density of states of the square lattice. Parameters: JS/t=24, n=0.7. The inset shows the low energy band of the spectrum on a smaller scale. Vertical lines indicate the chemical potential. The dash-dotted line in the inset is the Bloch-shaped FM ↑-QDOS ($S = 1/2$). The FM ↓-QDOS in this energy range practically vanishes (dotted line) indicating complete spin polarization.

QDOS in the inset of Fig. 3). For the ↑-electrons the localized moments act as an effective field and their quasiparticle density of states (QDOS) is merely the Bloch density of states shifted by $-\frac{1}{2}JS$. Within this picture the scaling by JS is expected to transfer directly to the total energy which is indeed the case as can be seen by the practically identical curves in Fig. 2 (right). In other words, the scaling of the FM energy with JS expresses the fact that spin waves are frozen.

The situation is different in the paramagnetic case. Now there are (energetically unfavored) states for ↑- and ↓-electrons with an antiparallel orientation to the localized spins. Whereas the lower energy band in Fig. 3 has a "parallel character" of localized and itinerant magnetic moment the upper band corresponds to an antiparallel orientation. As there are more eigenstates with a parallel spin-spin alignment one expects larger spectral weight of the corresponding peaks in the excitation spectrum. The lower the magnitude of the localized spin the higher this difference becomes: the parallel case "outweighs" the antiparallel case most dominantly for $S = 1/2$ ("triplet" vs. "singlet"). This can immediately be verified in the zero bandwidth limit.[24] There is indeed a higher spectral weight for low spin quantum numbers as can be seen in Fig. 3. On the other hand increasing S results in an equal distribution of spectral weight for both bands in the classical limit.[29] Thus, the paramagnetic state for lower magnitudes of the localized spins has lower total energy, as is observed in Fig. 2 (left).

Let us now proceed to the discussion of the magnetic phase diagrams we obtained in the spatial dimensions D =1,2, and 3. Fig. 4 shows the phase diagram in D = 1. The phase boundaries indicate the transition from FM to the phase separated FM-AFM regime except for the case $S = 1/2$ which gives a FM-PM transition. For comparison we added results by other authors obtained by numerical methods. Our findings give the same overall picture as earlier works with an increasing FM region as the Hund coupling becomes stronger. However we find that the $S = 1/2$-FKLM has a significantly reduced ferromagnetic stability due to its "early" transition to a PM state compared to higher localized spin quantum numbers. A second important feature is that we do not see any major differences in our phase boundaries for $S > 1/2$.

Our results compare well with the MC numerical phase diagram (classical spins) and with the DMRG results ($S = 3/2$). There is no considerable variation of the phase boundary for $S = 3/2$ and $S = \infty$ either.[12] The deviations are largest for $S = 1/2$: here our theory appears to underestimate the FM region. However, the authors of Ref. 18 attribute the fact that their FM region is reduced as compared to Ref. 13 to the higher number of lattice sites they include in their computation. Hence it would be desirable to have more DMRG results with larger system sizes to see how the phase boundaries change. We did not find a second transition from PM to PS for $S = 1/2$, neither did we take spiral or incommensurate correlations into account as was done in Ref. 18 and Ref. 13. However we can state that the reduction of the *maximal* region of FM for $S = 1/2$ with respect to

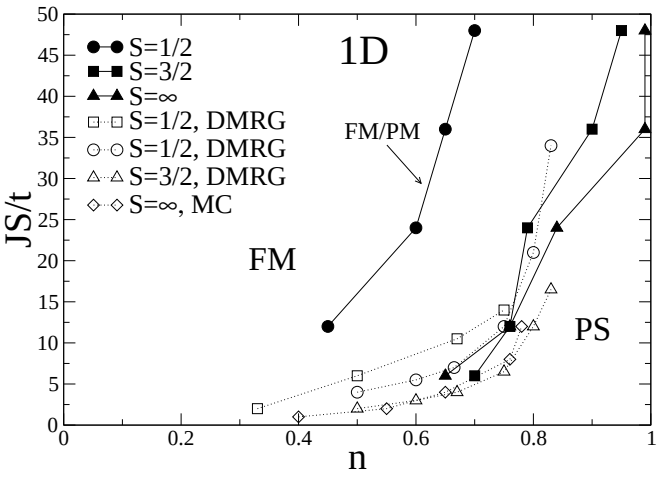

FIG. 4: Phase diagram in $D = 1$ for $S = \frac{1}{2}, \frac{3}{2}$ and classical spin. Filled symbols refer to our results and indicate the FM/PS transition ($S = 3/2, \infty$) and the FM/PM transition ($S = 1/2$). Open squares from Ref. 18 mark the transition from FM to a spiral phase; in this work an island phase between $n \approx 0.2$ and $n \approx 0.8$ and up to $JS/t \approx 8$, and PS for $n \geq 0.8$ and $JS/t \geq 10$ were also found. All other open symbols are taken from Ref. 13: circles ($S = 1/2$) and triangles ($S = 3/2$) indicate the boundary between FM and incommensurate correlations (IC), for $n \geq 0.8$ and above $JS/t \approx 12$ ($S = 1/2$) and $JS/t \approx 6$ ($S = 3/2$) PS was found, too; diamonds ($S = \infty$) mark transition from FM to PS ($JS/t \geq 4$) and from FM to IC at weaker coupling. Lines are guides to the eye.

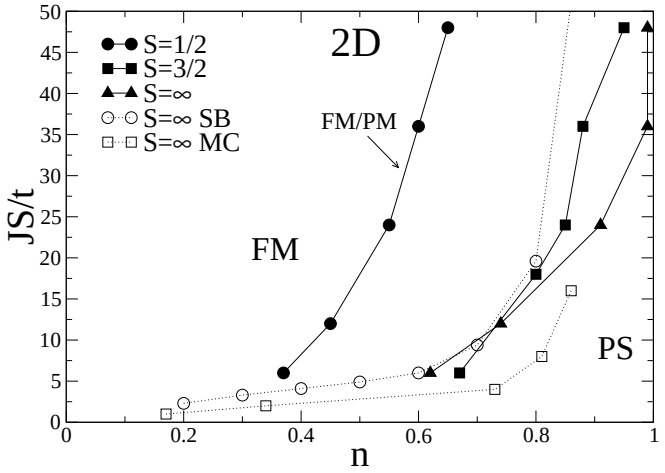

FIG. 5: Phase diagram in $D = 2$ for $S = \frac{1}{2}, \frac{3}{2}$ and classical spin. Open circles from Ref. 14 ($S = \infty$) indicate boundary between FM and PS above $JS/t \approx 7$ and between FM and a spiral phase at weaker coupling. SB stands for Schwinger-boson. Open squares from Ref. 12 ($S = \infty$) mark transition from FM to PS above $JS/t \approx 4$ and from FM to IC at weaker coupling. Lines are guides to the eye.

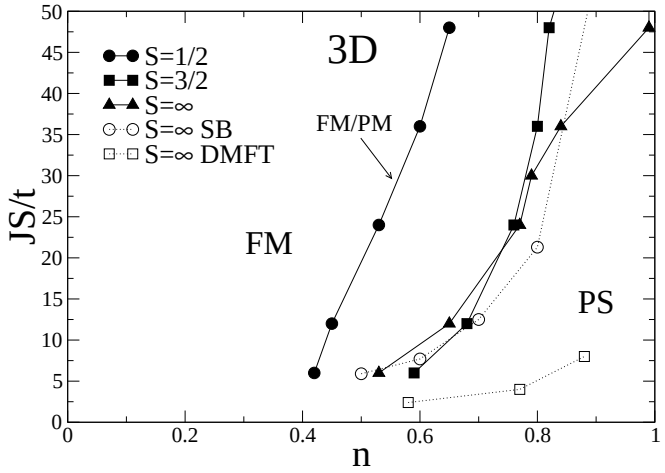

FIG. 6: Phase diagram in $D = 3$ for $S = \frac{1}{2}, \frac{3}{2}$ and classical spin. Open circles from Ref. 14 indicate boundary between FM and PS above $JS/t \approx 7$ and between FM and spiral phase at weaker coupling. Open squares from Ref. 11 (semicircular density of states) mark transition from FM to PS. Lines are guides to the eye.

higher spin quantum numbers is consistent with what we learn from the results obtained by other approaches.

Fig. 5 and 6 show the phase diagrams for 2D and 3D, respectively.[31] They give essentially the same picture as in 1D. Again we observe an unstability of the FM phase against PM for $S = 1/2$ only, reducing the region of FM stability as compared with higher S. There is no significant change of the phase boundary for $S > 1/2$ apart from some enhancement of FM for classical core spins and larger Hund couplings in all dimensions. The $S = \infty$ results in 2D are in accordance with MC simulations in Ref. 17 which yield FM for the full range of band filling at large J. We note a slight enlargement of the PS region in 3D for all S. However we do not want to emphasize the quantitative differences too much. As was already pointed out in Ref. 11 the small differences in the energies of the different phases lead to uncertainties in the exact location of the phase boundaries. In our case we estimate these error bars to be about 10% with respect to the corresponding electron density n. For the same reason we are careful not to put too much significance into the D-dependence of the crossing points of our $S = 3/2$ and classical S phase boundaries. However it is interesting to note that there is a crossing in all dimensions.

As before our findings agree well with those published by other authors who used different methods. There is one exception: compared to the other results the DMFT phase boundaries (however, for a $D = \infty$-Bethe lattice) from Ref. 11 seem to overestimate FM considerably.

We conclude that the magnetic properties of the FKLM at strong coupling and as far as the magnetic phases we investigated are concerned are rather insensitive to variations of the spatial dimension, at least at T=0. This falls in line with other results obtained using classical localized spins.[13]

IV. SUMMARY AND OUTLOOK

We have presented magnetic phase diagrams for the ferromagnetic Kondo lattice model in $D = 1, 2$, and 3. Our method is based on an equation of motion decoupling procedure fulfilling exact relations among Green functions and among their spectral moments. It does not require the assumption of classical spins. To determine the phase boundaries we computed and compared the total energy of the different phases at zero temperature.

There are three main results. First the case $S = 1/2$ appears to be special exhibiting a reduced region of ferromagnetism in the J-n-plane due to an instability of FM against spin disorder. Increasing the electron density this transition always takes place before FM/AFM phase separation can occur. Secondly the phase boundaries for $S > 1/2$ appear to be quite robust with respect to changes of the magnitude of the localized spin. This supports the widespread usage of classical localized spins in the treatment of the FKLM. Finally, these two features are recovered and quantitatively similar in the phase diagrams in all dimensions we investigated, namely 1D, 2D, and 3D.

To our knowledge there are no numerical phase diagram results in 2D and 3D with quantum localized spins as this is numerically a quite demanding task. It would be interesting to explore if the same trends as in 1D hold for $S = 1/2$ using numerically exact methods like DMRG.

It should also be a worthwhile task to examine the influence of the spin magnitude at higher temperatures up to the Curie temperature (in the vicinity of which colossal magnetoresistance occurs in the manganites). Phase boundaries may of course change to a certain extent with the crystal lattice structure, i.e. Bloch density of states. More changes can be expected when including a finite next-nearest neighbor hopping integral. Finally we focussed on the phases thought to be relevant for the intermediate to strong-coupling regime and left out other phases that come into play in the weak-coupling case. These issues are left for further investigation.

Appendix A: Interpolation coefficients

Exploiting spectral moment relations leads to the following coefficients in the approximations (17)-(20) for the higher order local Green functions:

$$\alpha_{1\sigma} = 0 \tag{25}$$

$$\beta_{1\sigma} = \frac{K_{1\sigma} + 4\Delta_{-\sigma} - 3z_\sigma\mu_{-\sigma} - \eta_\sigma}{\langle S^{-\sigma}S^\sigma\rangle + 2z_\sigma\Delta_{-\sigma} - \gamma_\sigma} \tag{26}$$

$$\alpha_{2\sigma} = \langle S^{-\sigma}S^\sigma\rangle - \beta_{2\sigma}\langle S^z\rangle \tag{27}$$

$$\beta_{2\sigma} = \frac{K_{2\sigma} + 2\eta_\sigma}{\langle (S^z)^2\rangle - \langle S^z\rangle^2 - \gamma_\sigma} \tag{28}$$

$$\alpha_{3\sigma} = -\gamma_\sigma \tag{29}$$

$$\beta_{3\sigma} = \frac{\mu_\sigma - z_\sigma\eta_\sigma + 2z_\sigma\vartheta + z_\sigma\gamma_\sigma\langle S^z\rangle}{\langle S^{-\sigma}S^\sigma\rangle + 2z_\sigma\Delta_{-\sigma} - \gamma_\sigma} \tag{30}$$

$$\alpha_{4\sigma} = \Delta_{-\sigma} + \beta_{4\sigma}\langle S^z\rangle \tag{31}$$

$$\beta_{4\sigma} = \frac{z_\sigma K_{3\sigma} - \mu_{-\sigma} - z_\sigma\eta_\sigma}{\langle (S^z)^2\rangle - \langle S^z\rangle^2 - \gamma_\sigma} \tag{32}$$

with the abbreviations:

$$K_{1\sigma} = 3z_\sigma\langle S^\sigma S^{-\sigma}\rangle + (S(S+1)-4)\langle S^z\rangle + z_\sigma\langle (S^z)^2\rangle - 2z_\sigma S(S+1)(1-\langle n_{-\sigma}\rangle) - \langle (S^z)^3\rangle \tag{33}$$

$$K_{2\sigma} = \left(S(S+1) - \langle S^{-\sigma}S^\sigma\rangle\right)\langle S^z\rangle - z_\sigma\langle (S^z)^2\rangle - \langle (S^z)^3\rangle \tag{34}$$

$$K_{3\sigma} = z_\sigma S(S+1)\langle n_{-\sigma}\rangle + \Delta_{-\sigma}(1 - z_\sigma\langle S^z\rangle) \tag{35}$$

The mixed expectation values

$$\gamma_\sigma = \langle S^{-\sigma}c_\sigma^\dagger c_{-\sigma}\rangle \tag{36}$$

$$\Delta_\sigma = \langle S^z n_\sigma\rangle \tag{37}$$

$$\mu_\sigma = \langle S^{-\sigma}S^\sigma n_\sigma\rangle \tag{38}$$

$$\eta_\sigma = \langle S^{-\sigma}S^z c_\sigma^\dagger c_{-\sigma}\rangle \tag{39}$$

$$\vartheta = \langle S^z n_\sigma n_{-\sigma}\rangle \tag{40}$$

can all be evaluated with the corresponding Green functions using the spectral theorem.

Appendix B: Localized spin expectation values

It holds for ferromagnetic saturation:

$$\langle (S^z)^2\rangle = S^2 \tag{41}$$

$$\langle (S^z)^3\rangle = S^3 \tag{42}$$

$$\langle S^{-\sigma}S^\sigma\rangle = S(1 - z_\sigma) \tag{43}$$

and for the paramagnetic phase:

$$\langle (S^z)^2\rangle = \frac{1}{3}S(S+1) \tag{44}$$

$$\langle (S^z)^3\rangle = 0 \tag{45}$$

$$\langle S^{-\sigma}S^\sigma\rangle = \frac{2}{3}S(S+1) \tag{46}$$

[1] C. Zener, Phys. Rev. **81**, 440 (1951); Phys. Rev. **82**, 403 (1951)
[2] P. W. Anderson and H. Hasegawa, Phys. Rev. **100**, 675 (1955)
[3] A. P. Ramirez, J. Phys.: Condens. Matter **9**, 8171 (1997)
[4] S. Satpathy, Z. S. Popovic, and F. R. Vukajlovic, Phys. Rev. Lett. **76**, 960 (1996)
[5] M. Quijada, J. Cerne, J. R. Simpson, H. D. Drew, K. H. Ahn, A. J. Millis, R. Shreekala, R. Ramesh, M. Rajeswari, and T. Venkatesan, Phys. Rev. B **58**, 16093 (1998)
[6] E. Dagotto, Nanoscale Phase Separation and Colossal Magnetoresistance, The Physics of Manganites and Related Compounds, Springer Series in Solid-State Sciences **136** (2003)
[7] H. Ohno, J. Magn. Magn. Mat. **200**, 110 (1999)
[8] I. Žutić, J. Fabian, and S. Das Sarma, Rev. Mod. Phys. **76**, 323 (2004)
[9] E. H. Hwang and S. Das Sarma, Phys. Rev. B **72**, 035210 (2005)
[10] K. Nagai, T. Momoi, and K. Kubo, J. Phys. Soc. Jpn. **69**, 1837 (2000)
[11] A. Chattopadhyay, A. J. Millis, and S. Das Sarma, Phys. Rev. B **64**, 012416 (2001)
[12] S. Yunoki, J. Hu, A. L. Malvezzi, A. Moreo, N. Furukawa, and E. Dagotto, Phys. Rev. Lett. **80**, 845 (1998)
[13] E. Dagotto, S. Yunoki, A. L. Malvezzi, A. Moreo, J. Hu, S. Capponi, D. Poilblanc, and N. Furukawa, Phys. Rev. B **58**, 6414 (1998)
[14] L. Yin, Phys. Rev. B **68**, 104433 (2003)
[15] M. Gulácsi, Adv. Phys. **53**, 769 (2004)

[16] D. Pekker, S. Mukhopadhyay, N. Trivedi, and P. M. Goldbart, Phys. Rev. B **72**, 075118 (2005)
[17] H. Aliaga, B. Normand, K. Hallberg, M. Avignon, and B. Alascio, Phys. Rev. B **64**, 024422 (2001)
[18] D. J. Garcia, K. Hallberg, B. Alascio, and M. Avignon, Phys. Rev. Lett. **93**, 177204 (2004)
[19] In the FKLM the total energy can be related to the local one-electron Green function. This is due to the bilinearity of the Hamiltonian in the fermionic operators. In other models, e.g. the Hubbard model, the corresponding formula is slightly more complicated and contains non-local terms.
[20] C. Santos and W. Nolting, Phys. Rev. B **65**, 144419 (2002)
[21] R. Schiller and W. Nolting, Phys. Rev. Lett. **86**, 3847 (2001)
[22] C. Santos, W. Nolting, and V. Eyert, Phys. Rev. B **69**, 214412 (2004)
[23] W. Nolting, S. Rex, and S. Mathi Jaya, J. Phys.: Condens. Matter **9**, 1301 (1997)
[24] W. Nolting, Grundkurs Theoretische Physik 7, Viel-Teilchen-Theorie, Springer Berlin (2005)
[25] W. Nolting, S. M. Jaya, and S. Rex, Phys. Rev. B **54**, 14455 (1996)
[26] By PS we always denote the coexistence of FM and AFM phases in the system.
[27] N. D. Mermin and H. Wagner, Phys. Rev. Lett. **17**, 1133 (1966)
[28] P. Fazekas, Lecture Notes on Electron Correlation and Magnetism, Series in Modern Condensed Matter Physics Vol. 5, World Scientific (1999)
[29] The different centers of gravity of the upper band are due to a different scaling behavior. In the zero bandwidth limit[24] the "antiparallel" excitation level scales as $J(S+1)$ rather than JS. In the framework of our theory the upper energy band can be interpreted in fact as a mixture of two bands, where one can be identified with the already mentioned parallel alignment of an electron and a localized magnetic moment and the other is linked to the break-up of a parallel coupling by a second conduction electron.[30]
[30] J. Kienert, "Das korrelierte Kondo-Gitter-Modell", Diplomarbeit, Humboldt-Universität zu Berlin (2001)
[31] We point out that the 2D results taken from Ref. 12 into Ref. 14 for comparison are larger than the originally published data by a factor 2.